Kinetic Inductance Detectors for the CADEx Experiment: Searching for Axions in the W-Band

David Rodriguez[1] · Marina C. de Ory[1] · Beatriz Aja[2] · Luisa de la Fuente[2] · Juan Daniel Gallego[3] · Enrique Villa[1] · Juan Pablo Pascual[2] · Eduardo Artal[2] · Daniel Granados[4] · Jesus Martin-Pintado[1] · Alicia Gomez[1]

Abstract
This paper presents the detector developments for the Canfrac Axion Detection Experiment (CADEx), aiming at detecting dark matter axions and dark photons within the W-band. A proof of concept of the detection system is based on an array of lumped-element kinetic inductance detectors (LEKIDs). Microstrip technology is used as read-out scheme, and the ground plane acts as backshort for optimizing optical absorption in the W-band. A titanium/aluminum bilayer is used for ensuring detection below 100 GHz. The detector array design includes an inner active section consisting of 36 detectors for direct detection of the axion signal and an additional outer rim of 28 blind pixels for calibration purposes. The nanofabrication process and a preliminary cryogenic characterization are presented, being the results in good agreement with the frequency design. Measured devices exhibit coupling quality factors of the order of 6×10^4, internal quality factors above 10^5 and an estimated kinetic inductance of 3.3 pH/□.

✉ David Rodriguez
  drodriguez@cab.inta-csic.es

✉ Alicia Gomez
  agomez@cab.inta-csic.es

1 Centro de Astrobiología (INTA-CSIC), Ctra. Torrejón-Ajalvir Km. 4, 28850 Torrejón de Ardoz, Spain

2 Departamento de Ingeniería de Comunicaciones, Universidad de Cantabria, 39005 Santander, Spain

3 Observatorio de Yebes, Centro de Desarrollos Tecnológicos (CDT), Instituto Geográfico Nacional (IGN), 19141 Yebes, Spain

4 IMDEA-Nanociencia, Cantoblanco, 28049 Madrid, Spain

1 Introduction to the CADEx Experiment

The Canfrac Axion Detection Experiment is a new proposal aiming at proving for the existence of the axions with a mass in the range of 330–460 µeV. The proposed system will use a haloscope placed in a very high magnetic field at a very low temperature (few tens of mK) for the axion–photon conversion and detecting photons in the W-band (75–110 GHz). The detection system is designed to measure the linearly polarized axion signal generated in the haloscope against the unpolarized background emission as a function of the resonance frequency of the haloscope [1]. Different state-of-the-art sensors have been assessed for the new generation of dark matter experiments including transition edge sensors, kinetic inductance detectors, single-nanowire single-photon-detectors or even quantum capacitance detectors [2]. CADEx, contrary to traditional dark matter experiments that use the axion spectral signature for its detection, takes advantage of the polarized fingerprint of the axion signal. Among the different detectors, kinetic inductance detectors have been chosen as baseline for the CADEx detection system. These detectors have already exhibited both extraordinary sensitivity, reaching noise equivalent power of 3×10^{-20} W/$\sqrt{\text{Hz}}$ [3], and performance in polarimetric astrophysics instruments [4, 5].

In this work, the preliminary developments of the W-band dual-polarization LEKIDs developed for CADEx are presented including microwave design, nanofabrication and low-temperature characterization.

2 LEKIDs Development for the CADEx Experiment

2.1 LEKIDs Design

The detector system is based on lumped-element kinetic inductance detectors, where the inductor acts as the effective absorber. Therefore, each pixel is a lumped element inductor–capacitance resonant circuit with a fixed inductor and a variable interdigital capacitor to allow frequency multiplexing. The LEKIDs are coupled to a microstrip line at a fixed distance to set the coupling factor for readout purposes. Figure 1 *Left* shows the proposed LEKID basic cell.

In our experiment, the high-frequency design of the LEKIDs maximizes the absorption of the inductor to the incoming radiation within the W-band for both polarizations. The inductor is configured in a 4th order Hilbert geometry, covering an area of 3.3×3.3 mm^2, with a strip width of 3 µm. The space-filling fractal Hilbert curve allows a constant filling factor over the detection area, guaranteeing a homogeneous optical coupling for both polarizations. The microstrip ground plane acts as the optical backshort, which maximizes the absorption in the W-band, in this case using 240 µm for the thickness of the silicon substrate.

The low-frequency design of the LEKIDs sets the resonance frequency (f_r), and the coupling quality factor (Q_c), to control the power delivered to the resonator
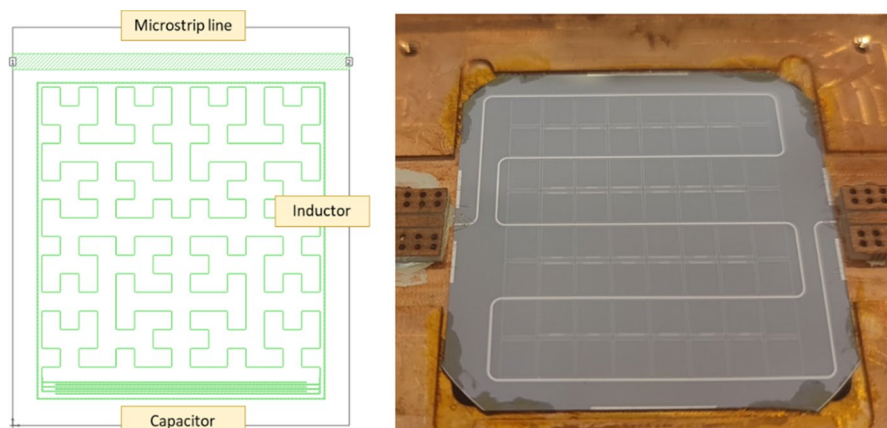
Fig. 1 *Left* schematic of a LEKID coupled to a microstrip read-out line, with the inductor and the interdigital capacitor. *Right* photograph of the 64 LEKIDs prototype fabricated on a silicon substrate of size 40×40 mm^2

for optimizing the dynamic range of the detector under millimeter wave radiation. The loaded quality factor of the resonator (Q) is given by $1/Q = 1/Q_i + 1/Q_c$, where Q_i is the internal quality factor. The coupling factor is chosen to avoid undercoupling regime ($Q_i < Q_c$) under illumination, where the detector visibility is degraded. As a $Q_i \approx 10^5$ is expected due to the 100 mK background in the CADEx experiment, the distance between the microstrip and the LEKIDs of 150 m is set to achieve a $Q_c = 5 \times 10^4$.

A design of 64 LEKIDs array is manufactured onto a 40×40 mm^2 wafer. The center area of the wafer (36 pixels), intended to measure the axion signal, uses 8-finger interdigital capacitors to set the resonance frequencies around 470 MHz. In the rim area, 28 detectors with 2-finger capacitors and resonance frequencies around 700 MHz are designed for background calibration purposes.

2.2 LEKIDs Nanofabrication

In order to absorb radiation within the W-band, the superconducting gap, and therefore the critical temperature (T_c), needs to be reduced below 1 K. For this purpose, the superconducting proximity effect is employed using a titanium/aluminum (Ti/Al) bilayer; where the reduction in T_c of the plain aluminum is achieved by adding a thin layer of a lower T_c superconductor (Ti) [6–8].

For the manufacturing, first, the substrate is treated with 1% hydrofluoric acid before deposition to reduce the two-level system (TLS) noise that limits the quality factor of the fabricated devices. Then, 15 nm of titanium and 15 nm of aluminum are deposited through a confocal sputtering system on a 240-µm-thick high-resistive silicon substrate. A T_c of 762 mK has been measured for this bilayer structure by DC transport characterization. Then, the design (microstrip line and resonators) is transferred to an AZ2070 nL of negative resist using maskless laser lithography and

to the bilayer structure using wet etching techniques. Subsequently, for the ground plane, a 200 nm of aluminum is deposited in the rear part of the wafer using DC sputtering. A final cleaning step based on an acetone and isopropanol bath is performed to obtain the final device. A photograph of the fabricated array is shown in Fig. 1 Right.

2.3 Dark Cryogenic Characterization

A cryogen-free dilution refrigerator with base temperature of 10 mK is used for cryogenic characterization. The complete harness set-up is fully described in Ref. [9]. The chip is assembled in a fully-enclosed holder to avoid any undesired radiation.

Figure 2 *Left* shows the S_{21} transmission parameter obtained under dark conditions at 10 mK with a read-out power of about -105 dBm in the detectors. Fifty-nine resonances out of 64 are found leading to a yield of 92% and at least a spacing of 98 kHz between the detectors is observed.

Figure 2 *Right* shows the resonance parameters obtained by following the calibration method explained in [10]. A mean $Q_c = 8.8 \times 10^4$ for the center detectors group (up to 560 MHz) whereas a mean $Q_c = 3.9 \times 10^4$ for the rim area (from 650 MHz). For all of them, a mean of $Q_c = 6.4 \times 10^4$ is obtained, and $Q_i = 6.2 \times 10^5$, which may be representative for the CADEx configuration as a background of 100 mK is expected. By comparing the resonant frequencies obtained from Sonnet simulations with the experimental ones, a kinetic inductance of $L_k = 3.3$ pH/□ is obtained leading to a kinetic fraction $\alpha = L_k/(L_k + L_g) = 0.52$.

Subsequently, a dark temperature response characterization is performed by sweeping the temperature of the mixing chamber in the refrigerator. Figure 3 Left shows the variation of one of the resonances when sweeping the bath temperature from 12 to 138 mK. As observed in Fig. 3 Right, both resonance frequency and quality factor are modified by sweeping temperature, which can be analyzed in terms of the variation of the complex conductivity of the superconductor studied with the Mattis–Bardeen model.
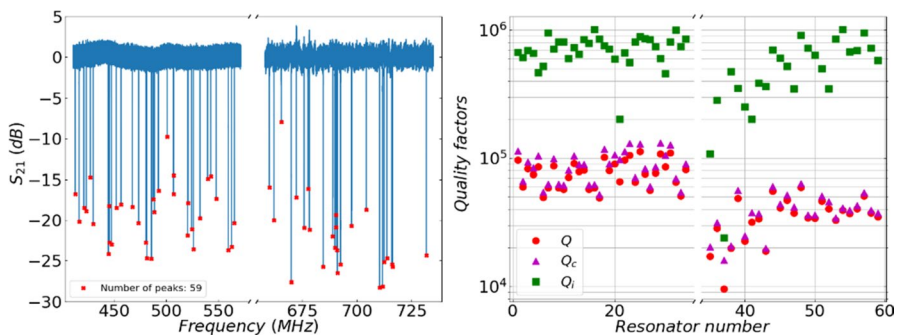

Fig. 2 *Left* measured resonances within the fabricated LEKID array. *Right* loaded (Q), internal (Q_i) and coupled (Q_c) quality factors for each fabricated pixel under dark conditions at T = 10 mK
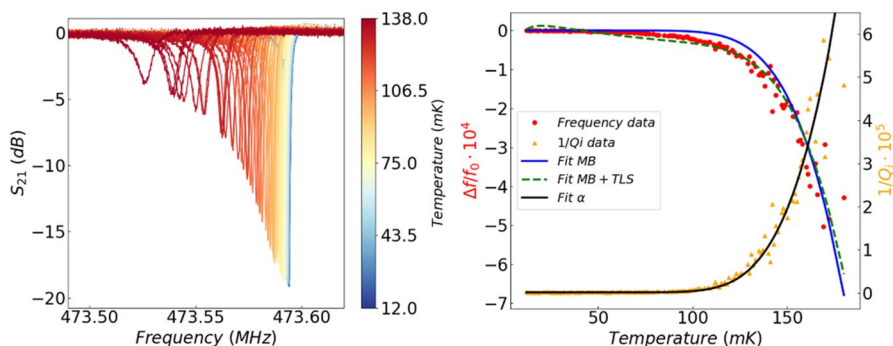
Fig. 3 *Left* resonance frequency of one LEKID for a temperature sweep between 12 and 138 mK. *Right* fractional change of the resonance frequency (red) and internal quality factor (yellow) as a function of temperature for the same LEKID. Different models are used to fit the experimental results

Black line shows the nonlinear fit to the internal quality factor evolution with temperature to $\frac{1}{Q_i} = \alpha \cdot \frac{\sigma_1}{\sigma_2} + \frac{1}{Q_{i,sat}}$, where σ_1 and σ_2 are the real and imaginary parts of the conductivity of the material. The best fitting results are obtained for $T_c = 768 \pm 31$ mK, $Q_{i,sat} = (4.43 \pm 0.18) \times 10^6$, and $\alpha = 0.60 \pm 0.18$.

The fractional change of the resonance frequency ($\Delta f = f_r - f_0$) can be described by a model that accounts for both the Mattis–Bardeen and *TLS* contributions [11]:

$$\left. \frac{\Delta f}{f_0} \right|_{TLS} = \frac{\alpha}{2} \cdot \frac{\Delta \sigma_2}{\sigma_2} - \frac{F \cdot \delta}{2} \cdot \frac{\Delta \epsilon}{\epsilon} \tag{1}$$

where δ is the characteristic dielectric loss called loss tangent, and F is a filling factor that accounts for the fraction of dielectric that fills the resonator volume. The fit green dashed line gives an $\alpha = 0.62 \pm 0.15$ and $T_c = 721 \pm 16$ mK. $F\delta = 2.77 \times 10^{-4} \pm 0.47 \times 10^{-4}$, which accounts for the TLS contribution, agrees to the previous studies of superconducting resonators fabricated on silicon substrates [11]. Discrepancies between the obtained α and T_c from the fits and the experimental characterization lay within the fitting error.

3 Conclusions

In this work, the developments of a superconducting LEKID camera to be employed as the detection system for the CADEx experiment are presented. It consists of a 64-pixel array of Ti/Al LEKIDs working within the W-band. The first experimental results agree with the designed quality factors and resonances, demonstrating a kinetic inductance of 3.3 pH/□ with average coupling and internal quality factors of 6.4×10^4 and 6.2×10^5, respectively. Further development is under progress for performing a full characterization of the LEKIDs in terms of the NEP.

Author Contributions D. R. and M. C. O. carried out the experimental work and the analysis of the results. All authors discussed the results and reviewed the manuscript which was led by A. G.

Declarations

Conflict of interest The authors declare no competing interests.

References

1. B. Aja et al., J. Cosmol. Astropart. Phys. Phys. **11**, 044 (2022). https://doi.org/10.1088/1475-7516/2022/11/044
2. J. Liu et al., Phys. Rev. Lett. **128**, 131801 (2022). https://doi.org/10.1103/PhysRevLett.128.131801
3. J.A. Baselmans et al., Astron. & Astrophys. **665**, A17 (2022). https://doi.org/10.1051/0004-6361/202243840
4. A. Ritacco et al., Astron. & Astrophys. **599**, A34 (2017). https://doi.org/10.1051/0004-6361/201629666
5. H. McCarrick et al., Astron. & Astrophys. **610**, A45 (2018). https://doi.org/10.1051/0004-6361/201732044
6. A. Catalano et al., Astron. & Astrophys. **580**, A15 (2015). https://doi.org/10.1051/0004-6361/201526206
7. A. Paiella et al., J. Low Temp. Phys. **184**, 97–102 (2016). https://doi.org/10.1007/s10909-015-1470-z
8. A. Paiella et al., J. Low Temp. Phys. **209**, 889–898 (2022). https://doi.org/10.1007/s10909-022-02848-z
9. B. Aja et al., IEEE Trans. Microw. Theory Tech. **69**(1), 578 (2021). https://doi.org/10.1109/TMTT.2020.3038777
10. S. Probst et al., Rev. Sci. Instrum. **86**, 024706 (2015). https://doi.org/10.1063/1.4907935
11. C.R.H. McRae et al., Rev. Sci. Instrum. **91**, 091101 (2022). https://doi.org/10.1063/5.0017378

Publisher's Note Springer Nature remains neutral with regard to jurisdictional claims in published maps and institutional affiliations.